ACS Catalysis

Research Article

pubs.acs.org/acscatalysis

Origins of Unusual Alcohol Selectivities over Mixed MgAl Oxide-Supported K/MoS_2 Catalysts for Higher Alcohol Synthesis from Syngas

Michael R. Morrill,[†] Nguyen Tien Thao,[†,¶] Heng Shou,[‡] Robert J. Davis,[‡] David G. Barton,[§] Daniela Ferrari,[⊥] Pradeep K. Agrawal,*[,†] and Christopher W. Jones*[,†]

[†]School of Chemical & Biomolecular Engineering, Georgia Institute of Technology, 311 Ferst Drive NW, Atlanta, Georgia 30332, United States

[‡]Chemical Engineering Department, University of Virginia, Charlottesville, Virginia 22904, United States

[§]Core R&D, The Dow Chemical Company, Midland, Michigan 48674, United States

[⊥]Hydrocarbons R&D, The Dow Chemical Company, 2301 North Brazosport Boulevard, Freeport, Texas 77451, United States

Supporting Information

ABSTRACT: A series of MoS_2 catalysts supported on Mg/Al hydrotalcite-derived mixed-metal oxide (MMO) supports promoted with K_2CO_3 is used for alcohol synthesis via CO hydrogenation. Alcohol selectivities are found to vary greatly when the Mo is loaded on the support at 5 wt % compared with 15 wt % Mo samples, all with a Mo/K atomic ratio of 1:1. The most striking difference between the catalysts is the comparatively low methanol and high C_{3+} alcohol selectivities and productivities achieved with the 5% Mo catalyst. This catalyst also produces more ethane than the 15% Mo catalyst, which is shown to be associated with ethanol dehydration and hydrogenation over residual acid sites on this catalyst with lower K content. A series of catalysts with common composition (5% Mo and 3% K supported on MMO) prepared in different manners all yield similar catalytic selectivities, thus showing that selectivity is predominately controlled by the MMO-to-Mo ratio rather than the synthesis method. When the Mo loading is the same, catalytic higher alcohol productivity shows some correlation to the degree of stacking of the MoS_2 layers, as assessed via X-ray diffraction and scanning transmission electron microscopy. Control reactions in which K loading is increased or the positioning of the MMO in the catalyst bed is changed via creation of multiple or mixed catalyst beds show that Mo/K/MMO domains play a significant role in alcohol-forming reactions. Higher alcohol-forming pathways are proposed to occur via CO insertion pathways or via coupling of adsorbed reaction intermediates at or near MoS_2 domains. No evidence is observed for significant alcohol-coupling pathways by adsorption of alcohols over downstream, bare MMO supports. Nitrogen physisorption, XRD, Raman, UV–vis DRS, STEM, and XANES are used to characterize the catalysts, demonstrating that the degree of stacking of the MoS_2 domains differs significantly between the low (5% Mo) and high (15% Mo) loading catalysts.

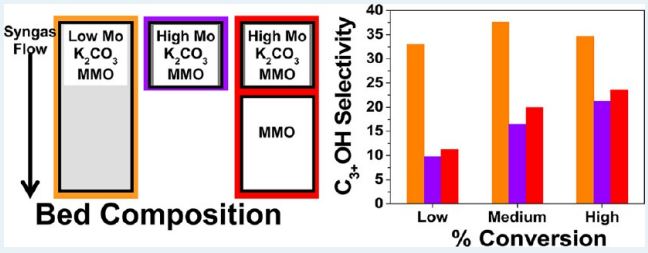

KEYWORDS: *syngas, higher alcohols, molybdenum sulfide, mixed metal oxide, hydrotalcite*

INTRODUCTION

Synthesis of methanol from syngas is a well-established commercial process, with significant understanding of the molecular level steps of the catalytic processes.[1−6] Higher alcohol synthesis, though not as thoroughly investigated as methanol synthesis, remains a topic of vigorous research since its initial significant investigation in the 1980s.[7−12] Higher alcohols such as ethanol can be produced via a variety of pathways, including sugar/lignocellulose fermentation, ethylene hydration, or the catalytic conversion of syngas (H_2, CO, and CO_2) via Fischer−Tropsch processes.[1−6,13] Along with ethanol, C_{3+} alcohols, such as 1-propanol and 1-butanol, are the focus of many studies because of their increasing use as fuel additives and chemicals.[7−12,14−16] Syngas conversion over solid catalysts based on a multitude of transition metals has been studied for this purpose, including Cu-, Fe-, Zn-, Ru-, Rh-, Mn-, and Mo-based compositions.[1−6,17−25]

Molybdenum sulfide-based catalysts, when combined with an alkali metal such as potassium,[7−12,26] are of particular interest because of their low cost compared with noble metal catalysts, their good alcohol selectivity, and their high resistance to sulfur poisoning. However, they also possess disadvantages, such as lower activity than noble metal catalysts and the need for comparatively higher reaction pressures to achieve useful catalytic productivities.[13,19,27−31] To reduce this disadvantage, promoters

Received: February 25, 2013
Revised: May 30, 2013
Published: June 5, 2013

   dx.doi.org/10.1021/cs400147d | ACS Catal. 2013, 3, 1665−1675

such as cobalt[9,11,12,14−16,32] have been added to increase alcohol selectivity, and nickel[33−35] has been used to improve catalytic activity.

In addition to bulk MoS_2-based catalysts, supported MoS_2 catalysts have also been widely evaluated as a means to maximize higher alcohol selectivity and productivity. Early studies were performed by Concha et al. and Tatsumi et al. using SiO_2, TiO_2, MgO, Al_2O_3, CeO_2, and a variety of carbons as supports.[10,36−38] Concha studied MoS_2 with no alkali addition, and Tatsumi studied reduced, oxidic Mo rather than MoS_2. Tatsumi et al. followed up their initial work with studies of Mo supported on silica, in which several olefins and alcohols were cofed into the reactant syngas stream.[39,40] They found added C_n olefins to yield higher amounts of C_{n+1} alcohols and concluded that CO insertion was the primary chain growth mechanism over these catalysts, rather than methanol homologation or alcohol coupling of lower alcohols (Guerbet reaction). Later, further studies were performed on MoS_2 using activated carbon,[11,41−46] multiwalled carbon nanotubes (MWCNT),[47−59] and γ-alumina[60−63] as supports.

Perhaps the two most important findings of the body of work on CO hydrogenation over supported MoS_2 are that dispersing MoS_2 domains greatly enhances catalytic activity and that the support itself can affect selectivity by facilitating other reaction pathways, some of which are unfavorable, such as alcohol dehydration. With these findings in mind, we recently investigated[64] the use of mesoporous Mg/Al mixed metal oxides (MMO) derived from layered double hydroxides[65−67] as a support to create dispersed MoS_2 domains for higher alcohol synthesis. We hypothesized that a more basic support would promote alcohol-forming reactions, unlike γ-alumina, which is commonly acidic and known instead to promote alcohol dehydration.[68−70] We found that the MMO support, when loaded with ∼5 wt % Mo and 3% K (Mo/K of 1:1), showed strikingly lower methanol selectivity than other supported catalysts, deviating from a typical Anderson Schulz Flory distribution, while maintaining a high C_{2+} alcohol selectivity at 8% CO conversion. In that report,[64] we postulated that the role of secondary reactions such as alcohol coupling could be a cause of the unusual alcohol distribution significantly biased toward C_{2+} alcohols.

Previous studies have shown that changes in Mo loading when supported on alumina can affect product distributions and activity for hydrogenation[43,71−73] and hydrodesulfurization[74] reactions. Most notably, Li et al. showed that increasing Mo loading on a carbon support led to decreased methanol-to-C_{2+}OH ratios and increased catalytic activities.[43] They attributed these outcomes to "more complete" Mo−K interactions that came about as Mo domains grew larger and Mo−support interactions became proportionately less prominent. In this study, we investigate the effects of Mo loading on MMO-supported catalysts in terms of selectivity and productivity. Additionally, we study the effects of K loading and the role of the MMO support to deconvolute the specific roles of Mo, K, and MMO in the reaction.

EXPERIMENTAL SECTION

MMO-supported catalysts with approximate Mo loadings of 5 and 15 wt % were synthesized and combined with K_2CO_3 (Sigma-Aldrich, 99%) in a manner similar to our previous study.[64] For this paper, the samples are referred to as Mo/K/MMO-5,3 (the first number, 5, denoting nominal Mo weight loading and the second number, 3, denoting K weight loading) and Mo/K/MMO-15,9, respectively. In brief, MMO was made via coprecipitation of a magnesium nitrate hexahydrate (Alfa Aesar, 98−102%) and aluminum nitrate nonahydrate (Alfa Aesar, 98−102%) aqueous solution (Mg/Al molar ratio of 7:3 and 0.6 M in metal ions) and with 1.2 M NaOH (EMD, 97.0%) and 0.15 M Na_2CO_3 (Aldrich, 99.5+ %) at 65 °C and a pH of 9.5. The solution was then stirred for 48 h, filtered, washed with deionized water, dried at 105 °C, then calcined at 450 °C for 2 h. Ammonium molybdate tetrahydrate (AMT) (Aldrich, ACS Reagent) was dissolved in DMSO (Aldrich, 99.9+ %) and added to MMO at room temperature via incipient wetness impregnation. DMSO was used as an impregnation solvent rather than water to prevent the partial reformation of the original hydrotalcite structure, which can, in turn, reduce catalytic activity by increasing crystallite size and "burying" promoters.[29,75,76] The material was then dried in open atmosphere at 135 °C for 12 h, loaded into a quartz tube, and decomposed via heating to 450 °C for 2 h with a heating rate of 5 °C/min under 40 mL/min of flowing nitrogen, which was used rather than air to maintain consistency with the previous study, which included carbon as a support.

Because of the low solubility of AMT in DMSO, the incipient wetness impregnation step was repeated multiple times to load adequate AMT onto the MMO support for Mo/K/MMO-15,9. After each impregnation, the sample was heated to 135 °C in open atmosphere for ∼12 h, then cooled to room temperature again. After the decomposition step (heating to 450 °C for 2 h), the resultant MoO_x/MMO samples were physically ground for 15 min with K_2CO_3 (Sigma-Aldrich, 99%, stored in an oven at 105 °C), pressed into 10 mm pellets at 1500 psig, crushed, and sieved to 20−40 mesh.

For catalytic reactions, sieved particles accounting for ∼50 mg Mo (1.0 g of a 5% Mo catalyst and 0.33 g of a 15% Mo catalyst) were loaded into a 1/4 in. steel tube and pretreated with 10% H_2S/H_2 (Matheson Tri-Gas, UHP) as described in our previous study.[64] Reactions with syngas, 45% H_2 (Airgas, UHP), 45% CO (Airgas, UHP, purified with 5A molecular sieve carbonyl trap), 10% N_2 (Airgas UHP) as an internal standard, and 50 ppm H_2S (from 5000 ppm H_2S in He, Matheson Tri-Gas, UHP) were carried out at 310 °C and 1500 psig at flow rates from ∼10 to 100 standard mL/min (700−17000 $mL_{syngas}/g_{catalyst}/h$). Reactions were carried out until activity and product selectivity stabilized, which took ∼4 days. Conversions were then changed as needed by changing syngas flow rate through the reactor. Please note that studies of toxic (CO, H_2S) and flammable (H_2, CO, H_2S) gases under high pressure require significant safety precautions.

An Agilent 7890 gas chromatograph was used to quantify the main reaction products (methane, ethane, ethylene, propane, propylene, butane, methanol, ethanol, 1-propaniol, isopropyl alcohol, 1-butanol, 2-methyl butanol, acetaldehyde, propionaldehyde, methyl formate, methyl acetate, and ethyl acetate). Details on product quantification may be found in a previous study.[64] The sulfide catalysts, oxide precatalysts, and supports were characterized via nitrogen physisorption, powder X-ray diffraction (XRD), Raman spectroscopy, UV−vis diffuse reflectance spectroscopy (DRS), extended X-ray absorption fine structure (EXAFS), X-ray absorption near edge spectroscopy (XANES), scanning transmission electron microscopy (STEM), and temperature-programmed reduction (TPR). Sulfided catalysts were characterized ex situ after in situ passivation with 1% O_2 in He (Matheson Trigas, UHP) for 8 h at room temperature flowing at 40 mL/min.

Elemental analysis was performed with a Perkin-Elmer Optima 7300 DV equipped with an optical emission spectrometer. Aliquots of each catalyst were digested in an H_2O_2/HNO_3 solution and then analyzed in duplicate. Nitrogen physisorption isotherms were collected at −196 °C using a Micromeritics Tristar II. All samples

dx.doi.org/10.1021/cs400147d | ACS Catal. 2013, 3, 1665−1675

were heated to 200 °C under vacuum for 10 h before analysis. XRD was performed using a Philips X-pert diffractometer using Cu Kα radiation.

Raman spectra were obtained using a Witec confocal Raman microscope (Alpha 300R) with an Ar^+ ion laser (λ = 514.5 nm) with 1 mW (for MoS_2) and 3 mW (for MoO_x) excitation source intensity. UV−vis spectra were obtained on a Cary UV−vis 500 with an internal diffuse reflectance cell. Pure MMO was used as a background. Samples for STEM were prepared by dispersing the particles in isopropyl alcohol, sonicating the dispersion, and dropping them on a TEM grid. Images were collected on a JEOL 2200FS-AC STEM operating at 200 keV at Oak Ridge National Laboratory.

X-ray absorption spectroscopy (EXAFS and XANES) was performed at beamlines X18B and X23A2 of the National Synchrotron Light Source (NSLS), Brookhaven National Laboratory. The storage ring was typically operated at 2.8 GeV with a ring current of ~300 mA. The XAS data were obtained in the transmission mode at the Mo K-edge (20 keV) with a spot size of 0.5 mm × 5 mm. The Mo K edge spectra were measured at room temperature in air with Mo foil (0.015 mm, 99.9%, Goodfellow) as energy references. Supported Mo samples were ground with boron nitride (99%, Aldrich) to obtain an absorption thickness of 1 inside a 5/32 in. i.d. pyrex tube. Three scans from 19 700 to 21 220 eV were collected for each sample. The XAS data were processed using the Athena[77] software for background removal, postedge normalization, and XANES analysis. Standard bulk MoS_2 (Acros, 98.5%) was used to determine the amplitude reduction factors (S_0^2) for Mo−S and Mo−Mo. The interatomic distances (r), coordination numbers (CN), Debye−Waller factors (σ^2), and energy shifts (ΔE_0) were derived from fitting the results in the Artemis software package.[77] The EXAFS results were fitted in R-space using two shells (Mo−S, Mo−Mo) generated theoretically using FEFF 6.0.[78]

RESULTS AND DISCUSSION

Catalyst Characterization. XRD patterns of the synthesized materials are shown in Figure 1. Diffraction lines that are characteristic of the MgO component of MMO at 44° and 64° were readily apparent on all supported samples. The lines are smaller on Mo/K/MMO-15,9 mostly likely due to disruption of MMO crystallinity on account of larger concentrations of Mo and K. A single diffraction line at 27° that corresponds to the (021) plane in MoO_3[79] can be observed only on the oxide precatalyst form of Mo/K/MMO-15,9. The Mo/K/MMO-5,3 counterpart does not show this diffraction line because the MMO support contains comparably smaller Mo domains. This difference is also reflected in the Raman and UV−vis spectra, which are discussed later in the text.

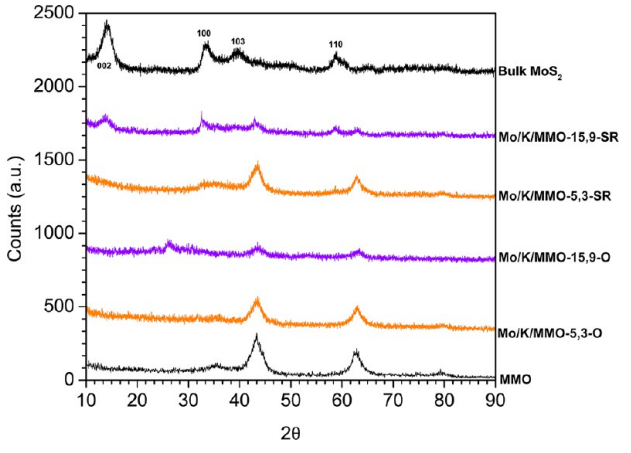

Figure 1. XRD of supported and unsupported K_2CO_3-promoted MoS_2. Supported samples were sulfided in situ and reacted with syngas for 2−4 days.

Both the oxide precatalyst forms of Mo/K/MMO-5,3 and Mo/K/MMO-15,9 show small peaks around 32° that are characteristic of potassium molybdate structures. Small peaks for the MoS_2 [100] (33°) and [110] (58°) planes were observed on both supported, sulfide samples. An interesting difference between the sulfide catalysts can be observed for the [002] plane of sulfide domains at 14°, which is prominent for the bulk MoS_2 sample, apparent for the Mo/K/MMO-15,9 catalyst, and absent for the Mo/K/MMO-5,3 catalyst. The presence of the line could be indicative of greater Mo−S stacking in the sulfided domains,[80] or because Mo loadings are different for the two catalysts, the peak's absence in Mo/K/MMO-5,3 could be attributed to the lower Mo loading.

The BET surface areas shown in Table 1 are calculated from nitrogen physisorption data and show a small drop when the MMO support was impregnated with 5% Mo and 3% K and a large drop in surface area when the support was impregnated with 15% Mo and 9% K. In addition, the Mo/K/MMO-5,3 sample lost much more surface area than Mo/K/MMO-15,9 after sulfidation and reaction. This effect may be due to a bigger impact of carbon deposition or sintering on the highly porous, exposed MMO surface of Mo/K/MMO-5,3 compared with the higher-loading Mo/K/MMO-15,9 sample.

Table 1. BET Surface Area Derived from Nitrogen Physisorption Data for the Materials Used in This Study

sample	BET surface area (m^2/g)
MMO support	209
Mo/K/MMO-5,3 − oxide precatalyst	151
Mo/K/MMO-5,3 − sulfided, reacted	69
Mo/K/MMO-15,9 − oxide precatalyst	26
Mo/K/MMO-15,9 − sulfided, reacted	24

The Raman spectra of the oxide precatalysts are shown in Figure 2a. The spectra of the oxide precatalysts were collected before the addition of K_2CO_3 to emphasize only the differences in the Mo domains. The 15% and 5% loaded Mo, alkali-free counterparts are denoted as Mo/MMO-15 and Mo/MMO-5, respectively. The Mo/MMO-15 spectrum showed bands at 957, 847, and 370 cm^{-1}. These bands are characteristic of $Mo_7O_{24}^{4-}$ domains that become increasingly prevalent when Mo loading rises.[81−83] Raman bands at bands 902 and 321 cm^{-1} are readily apparent for Mo/K/MMO-5 and are characteristic of MoO_4^{2-} domains. The band at 902 cm^{-1} is also present in the Mo/MMO-15 spectra, indicating that at high Mo loadings, a multitude of oxide domains will form.

Bands representing crystalline MoO_3 are absent from Mo/MMO-15, which has a Mo loading well above the monolayer surface coverage threshold. Notably, the sample itself was dark brown in color. These color centers have potential to scatter light and in turn mask characteristic bands. The sample's color is likely caused by a small amount of autoreduced Mo that formed during the decomposition of AMT. A second Raman spectrum was taken after treating Mo/MMO-5 and Mo/MMO-15 in a calcination oven in air at 450 °C for 2 h (Mo/MMO-5-Air and Mo/MMO-15-Air, respectively). The resultant spectrum shown in Figure S1 in the

dx.doi.org/10.1021/cs400147d | ACS Catal. 2013, 3, 1665−1675

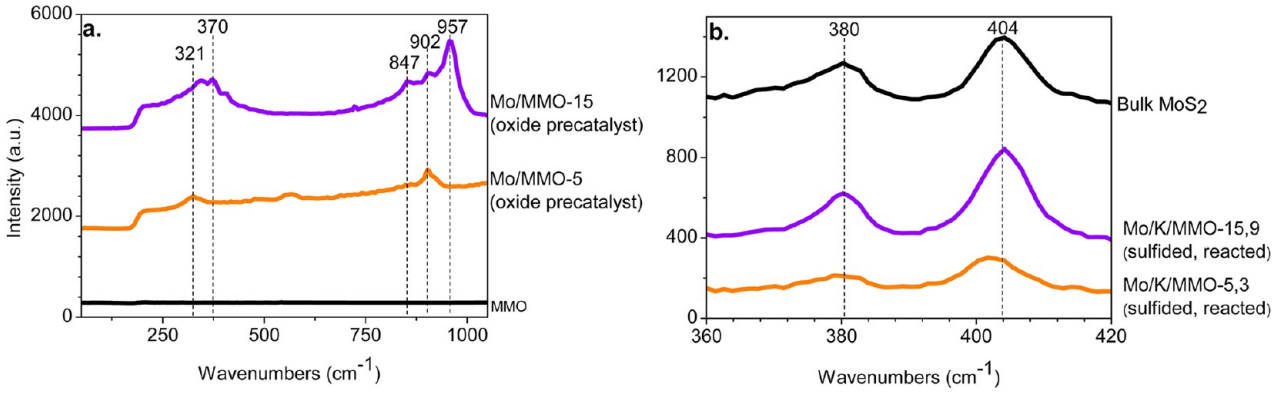

Figure 2. Raman spectra of the MMO supported Mo/K materials precatalysts (a) and sulfides (b) with a 1.5 and 0.5 mW 514 nm laser, respectively.

Supporting Information contains similar molybdate bands as Mo/MMO-15 and additional MoO_3 bands, as was originally expected. The autoreduced Mo likely existed in very small proportions, given the absence of MoO_2 character in both the XRD and XANES data. Specifically, the XRD pattern shows no MoO_2 diffraction lines, which implies that either crystalline MoO_2 is not present in the sample at all or that the domains are too small to be detected. The XANES spectrum, which will be discussed in more detail later, shows a K-edge that correlates almost perfectly with MoO_3. In addition, the band at 550 cm^{-1} on Mo/MMO-5, which correlates with neither MoO_2 nor MoO_3, disappeared on Mo/MMO-5-Air, indicating that it is not a likely component of the MoO_x structures.

Unlike in the case of the oxide precatalysts, the Raman spectra of the sulfided catalysts after reaction, shown in Figure 2b, do not show dramatic differences between the samples with different Mo loadings. Bands at 380 and 404 cm^{-1}, which are characteristic of Mo−S vibrations, were present in the two sulfide samples.[84] The implications of the Raman spectra of the sulfide samples is simply that the two catalysts possess similar Mo−S bonds that are not influenced differently by support interactions and that the peaks for the Mo−O vibrations have disappeared.

Additional information about the supported MoO_3 domains can be obtained from UV−vis DRS data.[85] The absorption edge energies of the various samples in this study were determined by plotting $[F(R_\infty)\ h\nu]^2$ vs $h\nu$ and then finding the x intercept of the line fitted to the low-energy rise of each spectrum in the data set. This rise represents a ligand-to-metal charge transfer whose energy is represented by the x intercept of the fit line.[81,83,85,86] Generally, lower energies are associated with larger aggregates. The UV−vis data in Figure 3 are complementary to the Raman spectra, yielding useful insights into the molybdenum domain sizes of the oxide precatalysts. The highest edge energy band of Mo/K/MMO-15 is between that of crystalline $Mo_7O_{24}^{6-}$ and $Mo_2O_7^{2-}$ standards from literature, whereas the edge energy for bulk MoO_3 is between that of MoO_3 and $Mo_7O_{24}^{6-}$.[85] Finally the edge energy of Mo/K/MMO-5 is close to that of crystalline MoO_4^{2-}. The spectra for Mo/MMO-15 has a second, less intense edge at ∼2.2 eV, which is absent from the UV−vis of Mo/MMO-15-Air shown in Figure S2 (Supporting Information). Consequently, this edge may be considered a mathematical artifact due to the dark color of the sample and extremely low reflectance.

The differences in the supported MoS_2 domains observed with XRD were clarified with STEM. Images of Mo/K/MMO-15,9 and Mo/K/MMO-5,3 are shown in Figure 4. Both samples have long, thin MoS_2 domains, but the structures in Mo/K/MMO-15,9 have approximately five stacked Mo−S layers, whereas

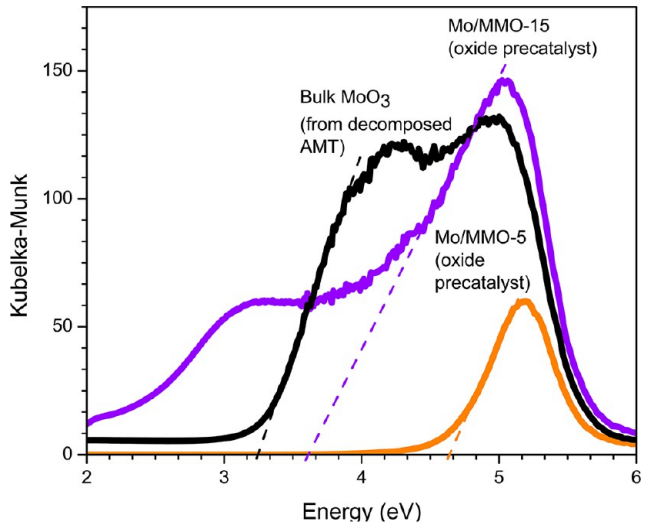

Figure 3. UV−vis DRS spectra for bulk MoO_3 (from decomposed AMT), Mo/MMO-15, and Mo/MMO-5.

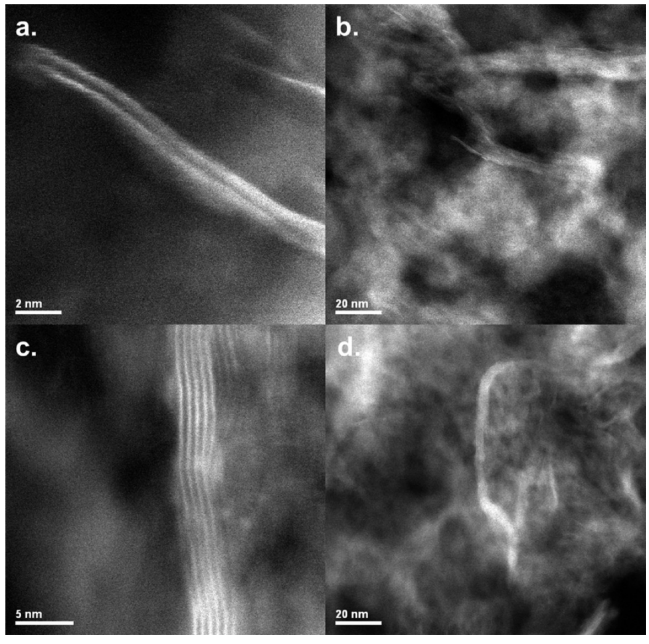

Figure 4. STEM images of Mo/K/MMO-5,3 (a and b) and Mo/K/MMO-15,9 (c and d) after sulfidation and reaction with syngas.

dx.doi.org/10.1021/cs400147d | ACS Catal. 2013, 3, 1665−1675

Mo/K/MMO-5,3 has about two. In addition, both of these samples have domains notably different from those observed in a bulk MoS_2 standard, which is made up of short, wide sheets with six or more Mo−S layers, as shown in Figure 5. The uniquely

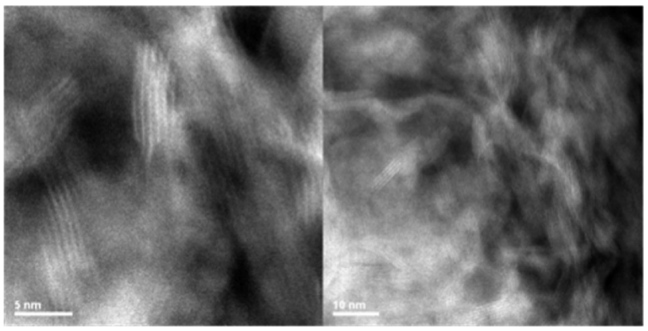

Figure 5. STEM images of bulk MoS_2 synthesized from ammonium molybdate tetrahydrate and ammonium sulfide.

different morphologies seen in the MMO-supported samples likely occur as a result of the differing initial Mo_yO_x domains, which according to the Raman and UV−vis spectra are (relatively) small on Mo/MMO-5 and larger on Mo/MMO-15.

The electronic and geometric structure of the molybdenum domains in the Mo/K/MMO-15,9 and Mo/K/MMO-5,3 samples can be further characterized by XANES spectra (Figure 6). XANES

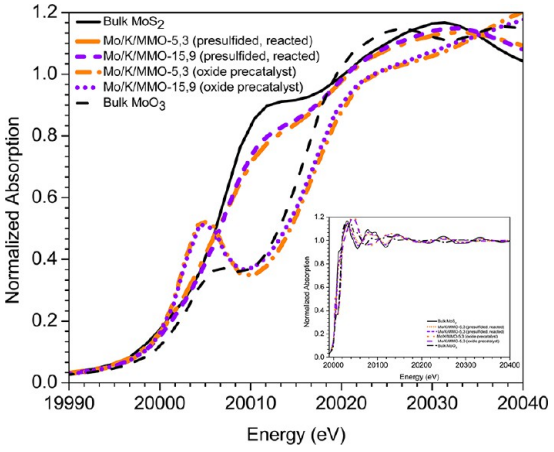

Figure 6. XANES Mo K-edge spectra of the 5% and 15% Mo supported MMO samples after combination with K_2CO_3, presulfidation, and reaction with CO.

has been used to provide insights into oxidation states and coordination environment.[24,87−91] This technique is specifically useful for assessing the state of Mo in the samples, as it may exist in catalysts and precatalysts in the form of MoO_2, MoO_3, and MoS_2, with each type of domain known to facilitate different reactions.[92−94] MoO_2 domains may exist as a product of incomplete sulfidation, which sometimes occurs when supports and promoters are added to a catalyst.[43] Previously, we have used XANES spectroscopy to characterize the state of the Mo species in supported catalysts, demonstrating that the XANES edge energy can be correlated with the electronic structure of the molybdenum.[20,95]

In the case of the catalysts investigated in this study, three important observations can be made from the XANES data. First, the two catalysts (Mo/K/MMO-5,3 and Mo/K/MMO-15,9) as oxides or sulfides closely resemble their bulk counterparts, which indicates fairly complete levels of oxidation or sulfidation, respectively, as opposed to significant oxysulfide content. Second, the two catalysts have indistinguishable edge energies when in the oxide form. As sulfides, they are also indistinguishable from one another. This outcome suggests that the average electronic structure of the Mo species is not affected by small differences in Mo domain structure. Finally, both the pre-edge and postedge features in the XANES spectra of the catalysts, as oxides or as sulfides, are also nearly identical. This outcome may be slightly unexpected in the case of the oxide precatalysts, given the differences revealed by UV−vis and Raman data. Specifically, one might expect the greater Mo−support interactions on Mo/K/MMO-5,3 than on Mo/K/MMO-15,9 in addition to the fundamentally different oxide domains (MoO_4^{2-} and $Mo_7O_{24}^{6-}$) to affect the K-edge. The most probable explanation for this observation is that the Mo^{VI}−O bonds are all similar in structure in these materials, regardless of whether the bonding oxygen atom comes from the oxide support or the Mo domain itself.

The Fourier transforms (FT) of k^3-weighted extended X-ray absorption fine structure (EXAFS) at the Mo K edge of bulk MoS_2 and the Mo/K/MMO samples after sulfidation and reaction are shown in Figure S3 (Supporting Information), and the structural parameters derived from the corresponding curve fits are presented in Table 2. Example curve fits associated with the results in Table 2 compared with the experimental EXAFS associated with Mo/K/MMO-15,9 (sulfided and reacted) are shown in Figure S4 (Supporting Information). All of the R factors of the fits are <0.04, indicating good agreement between the experimental EXAFS and the corresponding curve fits. The Mo−S and Mo−Mo interatomic distances in the supported MoS_2 samples (Mo/K/MMO-5,3 and Mo/K/MMO-15,9) matched that of bulk MoS_2 standard within experimental error, indicating that the supported Mo oxides were effectively sulfided in the supported samples, which is consistent with the XANES results (Figure 6). However, both of the supported sulfides presented a significantly lower Mo−Mo coordination number (~4) than that in bulk MoS_2 (6) and a greater Mo−Mo Debye−Waller factor ($\geq 3 \times 10^{-3}$ Å^2) than the corresponding value in bulk MoS_2 (1.9×10^{-3} Å^2), which indicates a high dispersion of Mo in the supported Mo sulfides.

The two-dimensional structure of a single MoS_2 layer has structural regularity consistent with a Mo−Mo coordination number of 6 within the layer. A reduced Mo−Mo coordination number of about 4 in the supported MoS_2 (Table 2) suggests that a single MoS_2 layer is truncated in one dimension and may be as small as two Mo atoms wide. Since the coordination number of Mo−Mo did not change upon increasing the Mo loading from 5 wt % to 15 wt %, the overall structure of the truncated layers must be quite similar. Because an increase in the number of stacked layers of a supported MoS_2 material is not expected to increase the coordination of the first Mo−Mo shell, it is unsurprising that the increase in number of MoS_2 "sheets" for Mo/K/MMO-5,3 and Mo/K/MMO-15,9 as was observed in STEM (Figure 4) had little effect on the Mo−Mo coordination numbers of the corresponding curve fits.

Effect of Mo and K Loading on Catalysis. Mo/K/MMO-5,3 and Mo/K/MMO-15,9 were synthesized and reacted with syngas at 310 °C and 1500 psig operating at 3−15% CO conversion. Linear alcohol and hydrocarbon selectivities for these catalysts are shown in Figures 7 and 8, respectively. These selectivities are presented on a CO_2-free basis for clarity, but it should be noted that MoS_2-based catalysts efficiently catalyze the water-gas shift reaction,[32,96−100] so CO_2 selectivities are high (see Table S2 in the Supporting Information). Two replicate batches for

dx.doi.org/10.1021/cs400147d | ACS Catal. 2013, 3, 1665−1675

Table 2. Results from the Analysis of Mo K Edge EXAFS[a]

sample	shell	CN	r (Å)	$\Delta\sigma^2$ (10^{-3} Å^2)	ΔE_0 (eV)	R factor
bulk MoS_2	Mo−S	6[b]	2.40 ± 0.01	2.3 ± 1.1	2.4 ± 1.0	0.028
	Mo−Mo	6[b]	3.14 ± 0.01	1.9 ± 1.2	−5.7 ± 1.6	
Mo/K/MMO-5,3, sulfided and reacted	Mo−S	5.2 ± 0.5	2.40 ± 0.01	3.0 ± 1.1	1.8 ± 1.0	0.033
	Mo−Mo	3.8 ± 1.5	3.13 ± 0.01	3.6 ± 2.0	−8.6 ± 2.3	
Mo/K/MMO-15,9, sulfided and reacted	Mo−S	4.9 ± 0.4	2.41 ± 0.01	2.6 ± 0.9	4.0 ± 0.9	0.031
	Mo−Mo	3.9 ± 1.2	3.13 ± 0.01	3.0 ± 1.4	−6.9 ± 1.9	

[a]Fitting parameters: Fourier transform range, Δk, 2−14.5 Å^{-1}; fitting range, ΔR, 1−3.2 Å; weighting, k^1 and k^3; S_0^2(Mo−S) = 0.84, S_0^2(Mo−Mo) = 0.79. [b]Value was assigned in curving-fitting on the basis of standard structure.

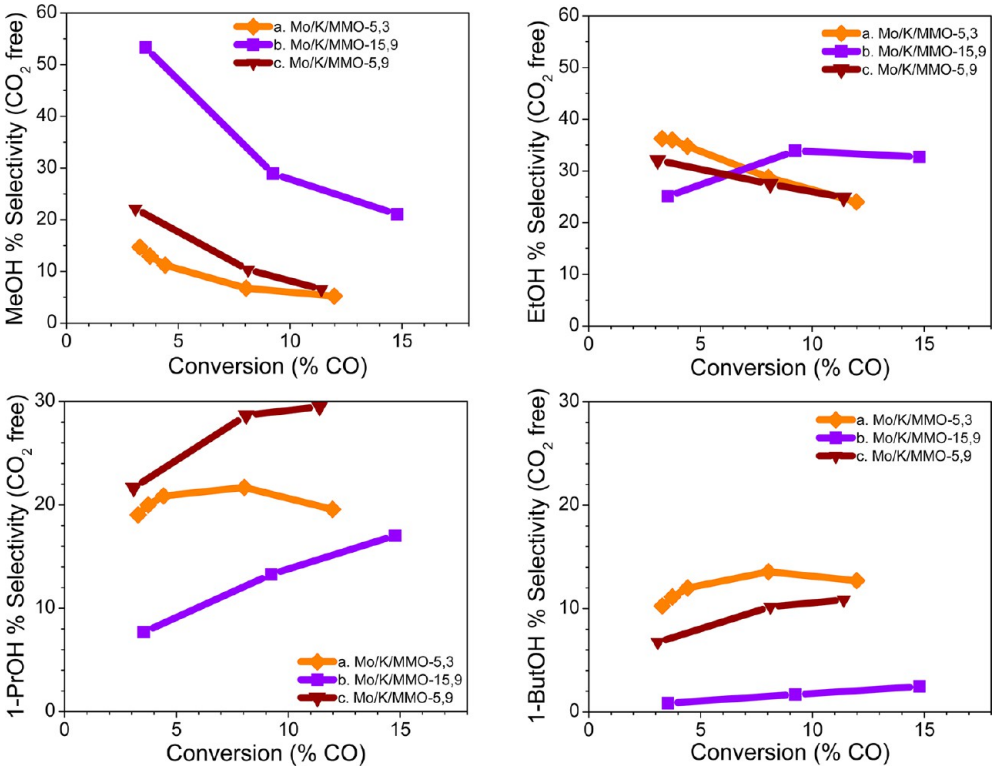

Figure 7. Alcohol selectivity (CO_2-free) vs CO conversion for C_1 to C_4 alcohols over MMO-supported catalysts, Mo/K/MMO-5,3, Mo/K/MMO-15,9, and Mo/K/MMO-5,9.

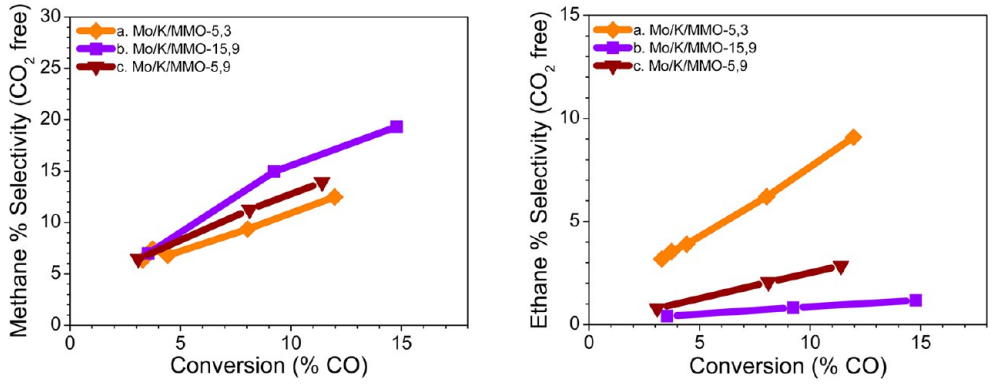

Figure 8. Alcohol selectivity (CO_2-free) vs CO conversion for methane and ethane over Mo/K/MMO-5,3, Mo/K/MMO-15,9, and Mo/K/MMO-5,9.

these catalysts were also synthesized and reacted to ensure consistency. The data with error bars are shown in Supporting Information Figures S5 and S6. In addition, as a control, Mo/K/MMO-5,3 was loaded with additional K such that the total K loading was the same as for Mo/K/MMO-15,9. Product selectivities for the resultant catalyst, Mo/K/MMO-5,9, are also shown in Figures 7 and 8.

Total selectivity for nonalcohol oxygenates (acetaldehyde, propionaldehyde, methyl formate, methyl acetate, and ethyl

dx.doi.org/10.1021/cs400147d | ACS Catal. 2013, 3, 1665−1675

acetate) are relatively small for all three catalysts, with selectivities at 1.9−2.3% for Mo/K/MMO-5,3, 1.8−3.1% for Mo/K/MMO-5,9, and 2.8−3.7% for Mo/K/MMO-15,9, indicating that oxygenate formation for these catalysts is chiefly linear, primary alcohols. With respect to linear hydrocarbons and alcohols, the two Mo/K/MMO-5,*x* catalysts show selectivity trends strikingly different from Mo/K/MMO-15,9. Specifically, methanol selectivities for Mo/K/MMO-5,*x* are substantially less than for Mo/K/MMO-15,9 at all conversions. Ethanol selectivity decreases with increasing conversion for Mo/K/MMO-5,*x* samples but increases with conversion for Mo/K/MMO-15,9. These outcomes suggest the selectivity differences are not related to K loading alone but are instead related to differences seen in the characterization data (i.e., differently sized MoS_2 domains) or high MMO/Mo ratios.

Ethane selectivity over these catalysts also emphasizes an important difference. There was little ethane production over the Mo/K/MMO-*x*,9 catalysts, but it was comparatively high over Mo/K/MMO-5,3. In addition to being a product of Fischer−Tropsch type CO insertions, ethane may also be a product of the dehydration of ethanol followed by hydrogenation of the produced olefin. The dehydration of alcohols is known to occur over acidic sites, such as those found on alumina, which is also a component of the MMO support. In a reducing environment, dehydration can be followed by hydrogenation, and thus, ethanol is converted to ethane, and 1-propanol, to propane. Because alcohols or their respective intermediates must first be formed for dehydration to take place, the reaction is likely secondary and should take place preferentially at higher conversions.

Indeed, ethane selectivity for Mo/K/MMO-5,3, as shown in Figure 8 and Supporting Information Table S2 (and propane selectivity, lumped with "Total HC" in Table S2) follow this expectation: increasing ethane selectivity with conversion. The Mo/K/MMO-*x*,9 catalysts, on the other hand, do not exhibit such behavior. Instead, these catalysts produce almost negligible amounts of C_{2+} hydrocarbons. This result is expected, given their high K content, which should neutralize acidic sites. Methanol is not likely involved in similar dehydration pathways, given the absence of dimethyl either, which was produced in quantities that were too small to be quantified. Ethylene was also notably absent from reaction products for all the catalysts, so assuming it is formed during ethanol dehydration, it must be quickly hydrogenated to ethane.

C_{3+} alcohol selectivity on Mo/K/MMO-5,9 surpasses that of Mo/K/MMO-5,3, which is expected and consistent with several studies that have quantified the effects of increasing K loadings on MoS_2 catalysts.[50,101,102] The interpretations of these studies (titration of acid sites and partial suppression of CO dissociation) do not, however, explain why the C_{3+} alcohol selectivity of Mo/K/MMO-5,3 is greater than that of Mo/K/MMO-15,9. In having a greater K loading and the same Mo/K ratio, the latter catalyst should have a more basic surface and therefore increasingly favor alcohol formation. The Mo/K/MMO-5,*x* catalyst must then have a character not directly related to K loading that also favors linear, primary alcohol formation over the formation of other oxygenates.

C_{3+} alcohol productivity ($g_{OH}/g_{Mo}/h$) is reported in Supporting Information Table S2 and shows a decrease with increasing CO conversion for the Mo/K/MMO-5,*x* catalysts but remains relatively constant for Mo/K/MMO-15,9. In addition, C_{3+} alcohol productivity for the Mo/K/MMO-5,*x* catalysts is more than twice that over Mo/K/MMO-15,9 at low conversions. These outcomes again suggest a fundamental difference in character between the catalysts that cannot be explained by differences in K loading alone.

Rather, this character is likely related to two key differences in catalyst structure: (i) variations in the proportion of surface-exposed MMO, Mo, and K and (ii) differences in MoS_2 structure, such as the stacking of the MoS_2 domains as reflected in XRD and STEM. On the basis of the data presented above, it is unknown what changes in selectivity either of these cases could bring about. Therefore, additional experiments were undertaken.

The first case would result if the MMO support served to promote reaction pathways different from K over a sulfide catalyst. Several papers in the literature show that MMO or MgO, a component in MMO, can couple alcohols in conjunction with other metals,[103−106] effectively making 1-propanol from methanol and ethanol, 1-butanol from 2 ethanols, and 2-methyl-propanol from 1-propanol and methanol. With that functionality, MMO could potentially perform a similar reaction over supported MoS_2 catalysts with or without the promotion of K. Alternatively, the interface of the MoS_2 domains with the MMO support could be important in the spillover and coupling of reactive intermediates between the various domains. Simply put, if MMO or MMO/Mo/K surfaces favor coupling of alcohols compared with MoS_2/K domains, a high MMO/Mo ratio would result in a bias toward C_{3+} alcohols not observed in the reaction of more conventional bulk MoS_2/K and, in parallel, a supported catalyst with high Mo content, as well.

Potential effects of the second case are more ambiguous. Several theoretical and experimental studies have linked differing edge geometries and coordinatively unsaturated site (CUS) numbers and spacings of the MoS_2 to active sites for CO or H_2 adsorption on MoS_2.[72,107−112] Thus, in addition to different CUS site structures, it is possible that different size MoS_2 domains could yield different active site concentrations that then lead to modified selectivities for higher alcohols. However, the precise effect of these different structures in the context of CO hydrogenation over supported MoS_2 is yet unknown. The following section provides an experimental pathway for deconvoluting both cases.

Role of MMO in Catalysis. To gain insight into the first case, namely, the functionality of MMO, bare MMO was combined with Mo in three different fashions for follow-up experiments. In the first experiment, sieved Mo/K/MMO-15,9 particles were placed upstream of a separate bed of identically sized bare MMO particles such that the total Mo, K, and MMO amounts were the same as in Mo/K/MMO-5,3 reaction (but with differing size and distribution of Mo and K domains). This reaction is referred to as Mo/K/MMO-15,9-MMOs. Figure 9d shows a schematic description of the catalyst bed for this experiment in addition to several others that will be discussed next.

For the second experiment, a mortar and pestle was used to grind the oxide precatalyst Mo/K/MMO-15,9 with bare MMO such that the total elemental composition of the resultant catalyst also matched that of Mo/K/MMO-5,3. This catalyst is referred to as Mo/K/MMO-15,9-MMOg (Figure 9e). The XRD patterns and BET surface area data of the oxide precatalyst and sulfided, reacted materials for these two cases are shown in Figure S7 and Table S1, respectively, in the Supporting Information. Notably, the XRD pattern for the Mo/K/MMO-15,9-MMOg precatalyst contained diffraction lines characteristic of molybdenum(VI) oxide and potassium molybdate at 27° and 32° respectively, which were similar in magnitude to those of Mo/K/MMO-15,9.

dx.doi.org/10.1021/cs400147d | ACS Catal. 2013, 3, 1665−1675

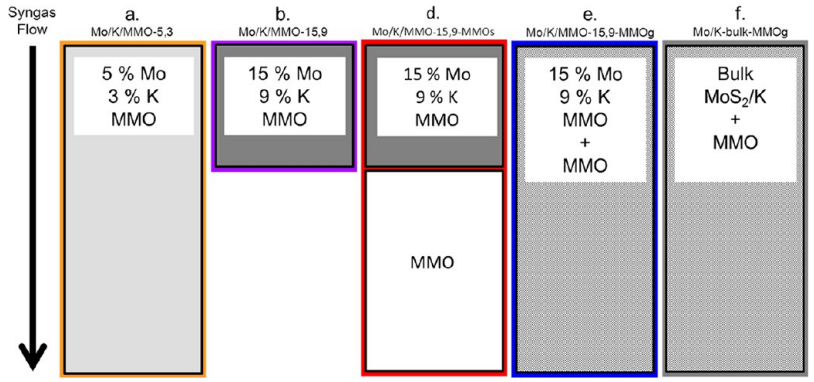

Figure 9. Catalyst bed schematics for Figures 7, 8, 10, and 11 showing various combinations of Mo, K, and MMO. Cases a and b represent the base cases for the study. Case c (not shown) represents the same catalyst as case a, but with a higher K content. Case d is the combination of catalyst b and bare MMO in series such that the final overall bed composition is the same as case a. Case e represents the same materials as case d, but ground into a homogeneous mixture. Case f was prepared similarly to e, but bulk MoS_2 was used as the Mo source instead of Mo/K/MMO-15,9. Cases a, d, e, and f represent catalyst beds with the same total amounts of MoS_2, K_2CO_3, and MMO in the bed.

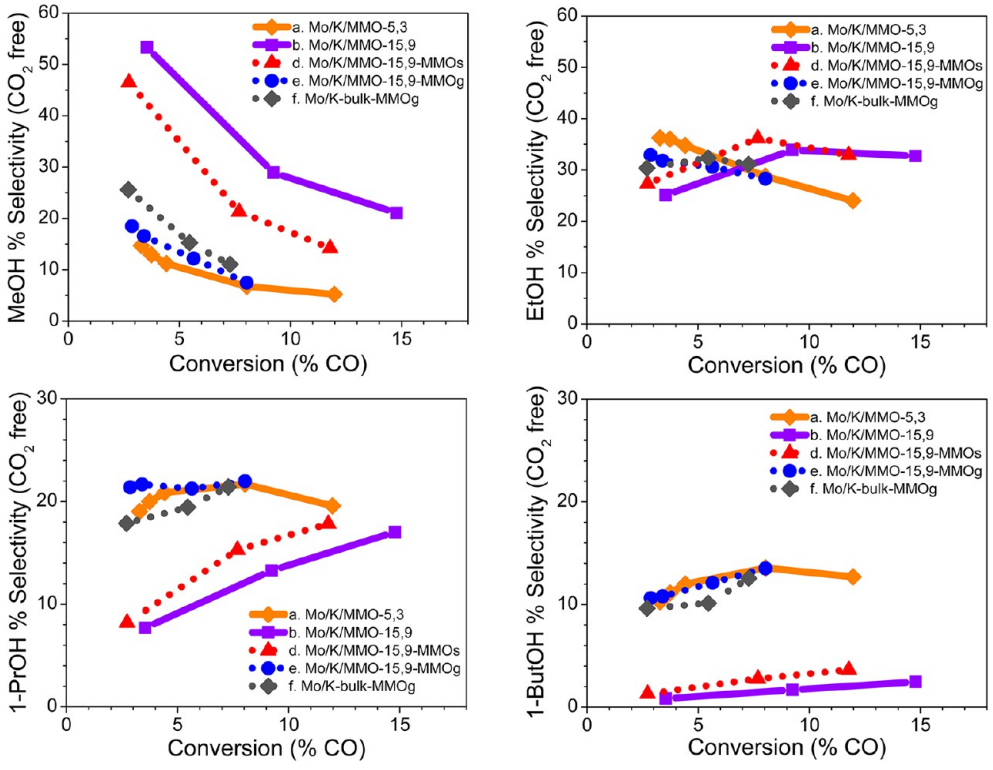

Figure 10. Alcohol selectivity (CO_2-free) vs CO conversion for C_1 to C_4 alcohols over MMO supported catalysts, Mo/K/MMO-5,3, Mo/K/MMO-15,9, Mo/K/MMO-15,9-MMOs, Mo/K/MMO-15,9-MMOg, and Mo/K-bulk-MMOg.

However, once sulfided and reacted, Mo/K/MMO-15,9-MMOg then showed XRD lines more similar to those of Mo/K/MMO-5,3: a short, broad peak (MoS_2) at 33° and two peaks (MgO) of much greater magnitude at 44° and 64°. This result suggests that initial oxide domain size does not, in fact, greatly affect sulfide domain size once the catalyst is sulfided. In other words, under sulfidation conditions, the Mo species can migrate around the support to a significant extent, to the point that the Mo/K/MMO-15,9-MMOg catalyst appears to have sulfide domains that are similar to the Mo/K/MMO-5,3 catalyst by XRD, despite very different preparation conditions. An extremely small peak at 14° correlating with the MoS_2 [002] plane can also be observed, indicating slightly more order in the stacking structure than in Mo/K/MMO-5,3. The overall Mo-to-MMO ratio in the precatalyst seems to play a dominant role in establishing the size of the MoS_2 domains.

Bulk MoS_2 (synthesized as described in the previous study[64]) was ground with bare MMO and K_2CO_3 to make the catalyst for the third and final experiment exploring the role of MMO, denoted as Mo/K-bulk-MMOg (Figure 9f). Despite the different Mo precursor, this catalyst had the same composition as the previous two: 85% MMO, 5% Mo, and 3% K. The XRD pattern for this catalyst shown in Figure S7 is similar to that of the sulfide form of Mo/K/MMO-15,9-MMOg, differing primarily in the magnitude of the peak at 14°, indicating a level of Mo−S stacking more closely resembling that of the original bulk (unsupported) catalyst.

Reactivity results for Mo/K/MMO-15,9-MMOs, Mo/K/MMO-15,9-MMOg, and Mo/K-bulk-MMOg are combined with those

dx.doi.org/10.1021/cs400147d | ACS Catal. 2013, 3, 1665−1675

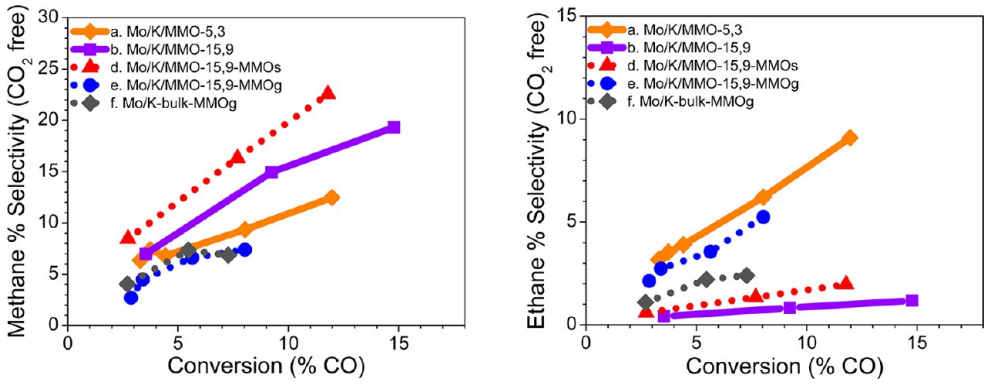

Figure 11. CO_2-free alcohol selectivity vs CO conversion for methane and ethane over MMO-supported catalysts Mo/K/MMO-5,3, Mo/K/MMO-15,9, Mo/K/MMO-15,9-MMOs, Mo/K/MMO-15,9-MMOg, and Mo/K-bulk-MMOg.

from Mo/K/MMO-5,3 and Mo/K/MMO-15,9 and shown in Figures 10 and 11 along with Table S2 in the Supporting Information. The trends of increasing methane and lowered methanol with increasing conversion can be observed for all five cases, which further strengthens the conclusions that methanol is a primary product of the reaction and is consumed via secondary reactions.[64]

The selectivity trends for the catalysts Mo/K/MMO-5,3, Mo/K/MMO-15,9-MMOg, and Mo/K-bulk-MMOg are shown to be virtually identical, despite the fact that the catalysts were generated via different synthesis routes (Mo/K/MMO-5,3 from a homogeneous mix of MMO, Mo, and K_2CO_3 with small MoO_x domains (Figure 9a); Mo/K/MMO-15,9-MMOg from the grinding of Mo/K/MMO-15,9, which has large MoO_x domains, and bare MMO (Figure 9e); and bulk MoS_2, K_2CO_3, and bare MMO (Figure 9f)). Specifically, the unusual trends associated with Mo/K/MMO-5,3 of lowered ethanol selectivity with increasing conversion and relatively high ethane selectivity were observed for Mo/K/MMO-15,9-MMOg and Mo/K-bulk-MMOg, but not for Mo/K/MMO-15,9-MMOs.

The fact that the low methanol selectivity observed over Mo/K/MMO-5,3[64] was not replicated by the Mo/K/MMO-15,9-MMOs experiment (with a downstream bare MMO bed) shows that the low methanol and high C_{3+}OH selectivity are not simply due to secondary reactions independently facilitated by bare MMO. If the low methanol and elevated higher alcohol selectivities over Mo/K/MMO-5,3 were associated with secondary reactions, they were likely not associated with conversion of stable products, such as methanol, into higher alcohols via alcohol coupling pathways (e.g., methanol + ethanol to give 1-propanol) over the bare, K-free support. These selectivity phenomena are likely instead related to reactions that occur only at an MMO−Mo−K interface or on MMO/K domains; both possibilities could result in adsorbed intermediates reacting to give the observed product distributions.

Thus, all the catalysts with an overall composition similar to Mo/K/MMO-5,3 gave similar catalytic selectivities, regardless of how they were prepared. Interestingly, however, the catalysts displayed different higher alcohol productivities. Specifically, of the three catalysts, Mo/K/MMO-5,3 showed the highest C_{3+}OH productivity (0.18 $g_{OH}/g_{Mo}/h$) at 8% CO conversion, whereas the two catalysts prepared via grinding (Mo/K-bulk-MMOg and Mo/K/MMO-15,9-MMOg) showed lower productivities (0.13 and 0.10 $g_{OH}/g_{Mo}/h$, respectively). The higher alcohol productivities (Supporting Information Table S2) appear to have some inverse correlation with the extent of the [002] peak at 14° 2θ in the XRD patterns (i.e., the absence of the peak correlates to greater higher alcohol productivity). Although the peaks are too small to be used in a line-broadening analysis,[80] at similar Mo loadings, a larger peak implies a higher level of orientation or MoS_2 slab stacking, as can be observed in the STEM images in Figures 4 and 5, where the bulk MoS_2 has the largest amount of stacking, and Mo/K/MMO-5,3, the least.

The effect of MMO on the reaction can perhaps most directly be observed by comparing C_4 alcohol selectivity for Mo/K/MMO-15,9 and Mo/K/MMO-15,9-MMOg. The addition of bare MMO to the former catalyst by dry impregnation resulted in over a 5-fold increase in 1-butanol selectivity and 3-fold increase in 2-methyl-1-propanol selectivity at 8% CO conversion. Although 1-butanol can be a product of insertion or coupling, 2-methyl-1-propanol is primarily hypothesized to be a product only of alcohol coupling. As such, relatively high 2-methyl-1-propanol selectivities provide a strong indicator of alcohol coupling pathways operating over some catalysts (Supporting Information Table S2).

It should be noted that the ethylene selectivity was low for all the reactions in this work (<1%). This outcome is especially significant for the Mo/K/MMO-15,9-MMOs experiment, which was designed to probe the role of the MMO support in catalyzing secondary reactions. If the MMO support dehydrated ethanol to produce ethylene over the Mo/K/MMO-5,3 catalyst, before olefin hydrogenation to yield ethane (as observed over this catalyst), it would be expected that the Mo/K/MMO-15,9-MMOs experiment would produce greater amounts of ethylene in the absence of a hydrogenating function in the second catalyst bed. The absence of ethylene in the Mo/K/MMO-15,9-MMOs product stream indicates that, similar to the discussion of the alcohol coupling pathways, bare MMO does not serve to dehydrate ethanol, producing ethylene and then ethane. Rather, dehydration, which is hypothesized to be the principal ethane formation pathway, must occur over acidic MoS_2 or MMO−Mo interface sites.

CONCLUSIONS

Two MMO-supported MoS_2 catalysts (Mo/K/MMO-5,3 and Mo/K/MMO-15,9) were used in CO hydrogenation to produce higher alcohols. The catalysts with low Mo loadings had MoS_2 domains containing the fewest layers and produced significantly higher amounts of C_{3+} alcohols and less methanol than the catalyst with the higher Mo loading. The catalyst with the lowest K loading (Mo/K/MMO-5,3) retained some residual acidity associated with the Mo/K/MMO domains that led to

dx.doi.org/10.1021/cs400147d | ACS Catal. 2013, 3, 1665−1675

significant ethane selectivity via ethanol dehydration and hydrogenation, whereas all other catalysts produced only small amounts of higher hydrocarbons, including ethane. Additional experiments using the Mo/K/MMO-15,9 catalyst followed by a second catalyst bed consisting of MMO demonstrated that the perturbed alcohol selectivities over the low Mo loading catalysts were associated primarily with reaction over the Mo domains over those catalysts, rather than via secondary reactions of readsorbed alcohols on MMO. A series of catalysts prepared with a common composition (akin to and Mo/K/MMO-5,3) but with different forms of Mo in the precatalyst (MoO_3, MoO_4^{2-}, $Mo_7O_{24}^{6-}$, MoS_2) all yielded similar catalytic selectivities, suggesting that the ratio of MMO to Mo determined the catalytic selectivity in the final sulfide catalysts. Catalytic productivity, on the other hand, appeared to be somewhat correlated with the degree of stacking of the MoS_2 domains, as evidenced by the intensity of the [002] reflection in XRD measurements and the observed degree of layer stacking from STEM images. Higher alcohol synthesis over these catalysts was associated with both CO insertion and oxygenate coupling reactions occurring with adsorbed intermediates on or near K/MoS_2 domains. Higher alcohol distributions suggest that some oxygenate coupling pathways may contribute to the observed products, especially at higher K loadings.

■ ASSOCIATED CONTENT

Supporting Information

Additional information as noted in text. This material is available free of charge via the Internet at http://pubs.acs.org.

■ AUTHOR INFORMATION

Corresponding Author

*E-mail: (P.K.A.) pradeep.agrawal@chbe.gatech.edu; (C.W.J.) cjones@chbe.gatech.edu.

Present Address

¶Faculty of Chemistry, Vietnam National University, 19-Le Thanh Tong ST, Hanoi, Vietnam

Notes

The authors declare no competing financial interest.

■ ACKNOWLEDGMENTS

This work was supported by The Dow Chemical Company. Use of the NSLS was supported by the U.S. Department of Energy, Office of Science, Office of Basic Energy Sciences, under Contract No. DE-AC02-98CH10886. Beamline X18B at the NSLS is supported in part by the Synchrotron Catalysis Consortium, U.S. Department of Energy Grant No. DE-FG02-05ER15688. The authors acknowledge with gratitude the invaluable assistance received from the X-23A2 beamline personnel, Dr. Bruce Ravel, and the X-18B beamline personnel, Dr. Nebojsa Marinkovic and Dr. Syed Khalid. Microscopy was supported by Oak Ridge National Laboratory's ShaRE User Facility, which is sponsored by the Office of Basic Energy Sciences, U.S. Department of Energy. The authors also wish to express special thanks to Dr. Kinga Unicoc for her assistance.

■ REFERENCES

(1) Natesakhawat, S.; Lekse, J. W.; Baltrus, J. P.; Ohodnicki, P. R., Jr.; Howard, B. H.; Deng, X.; Matranga, C. *ACS Catal.* **2012**, *2*, 1667−1676.

(2) Grabow, L. C.; Mavrikakis, M. *ACS Catal.* **2011**, *1*, 365−384.

(3) Yang, R.; Fu, Y.; Zhang, Y.; Tsubaki, N. *J. Catal.* **2004**, *228*, 23−35.

(4) Chinchen, G. C.; Denny, P. J.; Jennings, J. R.; Spencer, M. S.; Waugh, K. C. *Appl. Catal.* **1988**, *36*, 1−65.

(5) Solomon, E. I.; Jones, P. M.; May, J. A. *Chem. Rev.* **1993**, *93*, 2623−2644.

(6) Liu, X.-M.; Lu, G. Q.; Yan, Z.-F.; Beltramini, J. *Ind. Eng. Chem. Res.* **2003**, *42*, 6518−6530.

(7) Mazanec, T. J. *J. Catal.* **1986**, *98*, 115−125.

(8) Inoue, M.; Miyake, T.; Takegami, Y.; Inui, T. *Appl. Catal.* **1987**, *29*, 285−294.

(9) Stevens, R. R. *Process for Producing Alcohols From Synthesis Gas*; U.S. Patent 4752622, 1988.

(10) Tatsumi, T.; Muramatsu, A.; Tominaga, H. *Chem. Lett.* **1985**, 593−594.

(11) Murchison, C. B.; Conway, M. M.; Stevens, R. R.; Quarderer, G. J. In *9th Annual Congress on Catalysis*; Calgary, Alberta, Canada, 1988; pp 626−633.

(12) Santiesteban, J. G.; Bogdan, C. E.; Herman, R. G.; Klier, K. In *9th Annual Congress on Catalysis*, Calgary, Alberta, Canada, 1988; pp 561−568.

(13) Surisetty, V. R.; Dalai, A. K.; Kozinski, J. *Appl. Catal., A* **2011**, *404*, 1−11.

(14) Wu, M.; Wang, M.; Liu, J.; Huo, H. *Biotechnol. Prog.* **2008**, *24*, 1−11.

(15) Dernotte, J.; Mounaim-Rousselle, C.; Halter, F.; Seers, P. *Oil Gas Sci .Technol.* **2010**, *65*, 345−351.

(16) Balat, M.; Balat, H. *Appl. Energ.* **2009**, *86*, 2273−2282.

(17) Gupta, M.; Smith, M. L.; Spivey, J. J. *ACS Catal.* **2011**, *1*, 641−656.

(18) Subramani, V.; Gangwal, S. G. *Energy Fuels* **2008**, *22*, 814−839.

(19) Schwartz, V.; Campos, A.; Egbebi, A.; Spivey, J. J.; Overbury, S. H. *ACS Catal.* **2011**, *1*, 1298−1306.

(20) Shou, H.; Ferrari, D.; Barton, D. G.; Jones, C. W.; Davis, R. J. *ACS Catal.* **2012**, *2*, 1408−1416.

(21) Spivey, J. J.; Egbedi, A. *Chem. Soc. Rev.* **2007**, *36*, 1514−1528.

(22) Fang, K.; Li, D.; Lin, M.; Xiang, M.; Wei, W.; Sun, Y. *Catal. Today* **2009**, *147*, 133−138.

(23) Yang, Y.; Wang, Y.; Liu, S.; Song, Q.; Xie, Z.; Gao, Z. *Catal. Lett.* **2009**, *127*, 448−455.

(24) Gogate, M. R.; Davis, R. J. *ChemCatChem.* **2009**, *1*, 295−303.

(25) Gao, J.; Mo, X.; Chien, A. C.-Y.; Torres, W.; Goodwin, J. G., Jr. *J. Catal.* **2009**, *262*, 119−126.

(26) Lee, J. S.; Kim, S.; Lee, K. H.; Nam, I. S.; Chung, J. S.; Kim, Y. G.; Woo, H. C. *Appl. Catal., A* **1994**, *110*, 11−25.

(27) Nunan, J. G.; Bogdan, C. E.; Klier, K.; Smith, K. J.; Young, C. W.; Herman, R. G. *J. Catal.* **1988**, *113*, 410−433.

(28) Nunan, J. G.; Bogdan, C. E.; Klier, K.; Smith, K. J.; Young, C.; Herman, R. G. *J. Catal.* **1989**, *116*, 195−221.

(29) Nunan, J. G.; Herman, R. G.; Klier, K. *J. Catal.* **1989**, *116*, 222−229.

(30) Haider, M. A.; Gogate, M. R.; Davis, R. J. *J. Catal.* **2009**, *261*, 9−16.

(31) Arakawa, H.; Fukushima, T.; Ichikawa, M.; Natsushita, S.; Takeuchi, K.; Matsuzaki, T.; Sugi, Y. *Chem. Lett.* **1985**, *7*, 881−884.

(32) Chen, Y.; Dong, M.; Wang, J.; Jioa, H. *J. Phys. Chem. B* **2010**, *114*, 16660−16676.

(33) Li, D.; Yang, C.; Qi, H.; Zhang, H.; Li, W.; Sun, Y.; Zhong, B. *Catal. Commun.* **2004**, *5*.

(34) Li, D.; Yang, C.; Li, W.; Sun, Y.; Zhong, B. *Top. Catal.* **2005**, *32*, 233−239.

(35) Li, D.; Yang, C.; Zhao, N.; Qi, H.; Li, W.; Yuhan, S.; Zhong, B. *Fuel Proc. Technol.* **2007**, *88*, 125−127.

(36) Tatsumi, T.; Muramatsu, A.; Tominaga, H. *Appl. Catal.* **1986**, *27*, 69−82.

(37) Tatsumi, T.; Muramatsu, A.; Tominaga, H. *Appl. Catal.* **1987**, *34*, 77−88.

(38) Concha, B. E.; Bartholomew, G. L.; Bartholomew, C. H. *J. Catal.* **1984**, *89*, 536−541.

(39) Tatsumi, T.; Muramatsu, A.; Yokota, K.; Tominaga, H. *J. Catal.* **1989**, *115*, 388−398.

(40) Tatsumi, T.; Muramatsu, A.; Yokota, K.; Tominaga, H. *J. Mol. Catal.* **1987**, *41*, 385−389.
(41) Li, X.; Feng, L.; Zhang, L.; Dadyburjor, D. B.; Kugler, E. L. *Molecules* **2003**, *8*, 13−30.
(42) Li, X.; Feng, L.; Lui, Z.; Zhong, B.; Dadyburjor, D. B.; Kugler, E. L. *Ind. Eng. Chem. Res.* **1998**, *37*, 3853−3863.
(43) Li, Z.-R.; Jiang, M.; Hu, T.-D.; Lui, T.; Xie, Y.-N. *J. Catal.* **2001**, *199*, 155−161.
(44) Iranmahboob, J.; Hill, D. O. *Catal. Lett.* **2002**, *78*, 49−55.
(45) Gang, L.; Chengfang, Z.; Yanqing, C.; Zhibin, Z.; Yianhui, N.; Linjun, C.; Fong, Y. *Appl. Catal., A* **1997**, *150*, 243−252.
(46) Duchet, J. C.; Van Oers, E. M.; De Beer, H. J.; Pruins, R. *J. Catal.* **1983**, *89*, 386−402.
(47) Ma, X.; Lin, G.; Zhange, H. *Catal. Lett.* **2006**, *111*, 141−151.
(48) Ma, X.; Goudong, L.; Hongbin, Z. *Chin. J. Catal.* **2006**, *27*, 1019−1027.
(49) Ma, C.-H.; Li, H.-Y.; Lin, G.-D. *Catal. Lett.* **2010**.
(50) Surisetty, V. R.; Tavasoli, A.; Dalai, A. K. *Appl. Catal., A* **2009**, *365*, 243−251.
(51) Surisetty, V. R.; Dalai, A. K.; Kozinski, J. *Ind. Eng. Chem. Res.* **2010**, *49*, 6956−6963.
(52) Surisetty, V. R.; Dalai, A. K.; Kozinski, J. *Appl. Catal., A* **2010**, *385*, 153−162.
(53) Surisetty, V. R.; Dalai, A. K.; Kozinski, J. *Appl. Catal., A* **2010**, *381*, 282−288.
(54) Surisetty, V. R.; Dalai, A. K.; Kozinski, J. *Energy Fuels* **2010**, *24*, 4130−4137.
(55) Surisetty, V. R.; Dalai, A. K.; Kozinski, J. *Appl. Catal., A* **2011**, *393*, 50−58.
(56) Surisetty, V. R.; Dalai, A. K.; Kozinski, J. *Energy Fuels* **2011**, *25*, 580−590.
(57) Surisetty, V. R.; Kozinski, J.; Dalai, A. K. *Int. J. Chem. React. Eng.* **2011**, *9*, 1−18.
(58) Surisetty, V. R.; Eswaramoorthi, I.; Dalai, A. K. *Fuel* **2012**, *96*, 77−84.
(59) Surisetty, V. R.; Epelde, E.; Dalai, A. K.; Trepanier, M.; Kozinski, J. *Int. J. Chem. React. Eng.* **2012**, *10*, 1−15.
(60) Li, Z.-R.; Fu, Y.-L.; Jiang, M. *Appl. Catal., A* **1999**, *187*, 187−198.
(61) Li, Z.; Fu, Y.-L.; Jiang, M.; Meng, M.; Xie, Y.-N.; Hu, T.-D.; Lui, T. *Catal. Lett.* **2000**, *65*, 43−48.
(62) Fu, Y.; Fujimoto, K.; Lin, P.; Omata, K.; Yu, Y. *Appl. Catal., A* **1995**, *126*, 273−285.
(63) Bian, G.; Fu, Y.; Ma, Y. *Catal. Today* **1999**, *51*, 187−193.
(64) Morrill, M. R.; Thao, N. T.; Agrawal, P. K.; Jones, C. W.; Davis, R. J.; Shou, H.; Barton, D. G.; Ferrari, D. *Catal. Lett.* **2012**, *142*, 875−881.
(65) Valente, J. *J. Catal.* **2000**, *189*, 370−381.
(66) Fishel, C. T.; Davis, R. J. *Catal. Lett.* **1994**, *25*, 87−95.
(67) Bezen, M. C. I.; Breitkopf, C.; Lercher, J. A. *ACS Catal.* **2011**, *1*, 1384−1393.
(68) Arai, H.; Take, J.; Saito, Y.; Yoneda, Y. *J. Catal.* **1967**, *9*, 146−153.
(69) Golay, S.; Doepper, R.; Renken, A. *Appl. Catal., A* **1998**, *172*, 97−106.
(70) Bautista, F. M.; Delmon, B. *Appl. Catal., A* **1995**, *1995*, 47−65.
(71) Jalowiecki-Duhamel, L.; Grimblot, J.; Bonnelle, J. P. *J. Catal.* **1991**, *129*, 511−518.
(72) Kasztelan, S.; Toulhoat, H.; Grimblot, J.; Bonnelle, J. P. *Appl. Catal.* **1984**, *13*, 127−159.
(73) Bian, G.-Z.; Fan, L.; Fu, Y.-L.; Fujimoto, K. *Appl. Catal., A* **1998**, *170*, 255−268.
(74) Bachelier, J.; Tilliette, M. J.; Duchet, J. C.; Cornet, D. *J. Catal.* **1982**, *76*, 300−315.
(75) Takehira, K. *Catal. Commun.* **2004**, *5*, 209−213.
(76) Perez-Ramirez, J.; Abello, S.; van der Pers, N. M. *Chem.—Eur. J.* **2007**, *13*, 870−878.
(77) Ravel, B.; Newville, M. *J. Synchrotron Radiat.* **2005**, *12*, 537−541.
(78) Zabinsky, S. I.; Rehr, J. J.; Ankudinov, A.; Albers, R. C.; Eller, M. J. *Phys. Rev. B* **1995**, *52*, 2995−3009.
(79) Ressler, T. *J. Catal.* **2002**, *210*, 67−83.
(80) Liang, K. S.; Chianelli, R.; Chien, F. Z.; Moss, S. C. *J. Non-Cryst. Solids* **1986**, *79*, 251−273.
(81) Lee, E. L.; Wachs, I. E. *J. Phys. Chem. C* **2007**, *111*, 14410−14425.
(82) Wachs, I. E.; Roberts, C. A. *Chem. Soc. Rev.* **2010**, *39*, 5002.
(83) Tian, H.; Roberts, C. A.; Wachs, I. E. *J. Phys. Chem. C* **2010**, *114*, 14110−14120.
(84) Muller, A.; Weber, T. *Appl. Catal.* **1991**, *77*, 243−250.
(85) Weber. *J. Catal.* **1995**, *151*, 470−474.
(86) Gao, X. *J. Catal.* **2002**, *209*, 43−50.
(87) Wilke, M.; Partzsch, G. M.; Bernhardt, R.; Lattard, D. *Chem. Geol.* **2004**, *213*, 71−87.
(88) Wilke, M.; Farges, F.; Petit, P.; Brown, G. E.; Martin, F. *Am. Mineral.* **2001**, *86*, 714−730.
(89) Millet, J. M. M.; Baca, M.; Pigamo, A.; Vitry, D.; Ueda, W.; Dubois, J. L. *Appl. Catal., A* **2003**, *244*, 359−370.
(90) Mountjoy, G.; Pickup, D. M.; Wallidge, G. W.; Anderson, R.; Cole, J. M.; Newport, R. J.; Smith, M. E. *Chem. Mater.* **1999**, *11*, 1253−1258.
(91) Farges, F.; Brown, G. E.; Rehr, J. J. *Phys. Rev. B* **1997**, *56*, 1809−1819.
(92) Chisholm, M. H.; Folting, K.; Huffman, J. C.; Kirkpatrick, C. C. *Inorg. Chem.* **1984**, *23*, 1021−1037.
(93) Delporte, P.; Huu-Pham, C.; Ledoux, M. J. *Appl. Catal., A* **1997**, *149*, 151−180.
(94) Pecoraro, T. A.; Chianelli, R. *J. Catal.* **1981**, 430−445.
(95) Li, L.; Morrill, M. R.; Shou, H.; Barton, D. G.; Ferrari, D.; Davis, R. J.; Agrawal, P. K.; Jones, C. W.; Sholl, D. S. *J. Phys. Chem. C* **2013**, *117*, 2769−2773.
(96) Hou, P.; Meeker, D.; Wise, H. *J. Catal.* **1983**, *80*, 280−285.
(97) X, S.; Wang, S.; Hu, J.; Wang, H.; Chen, Y.; Qin, Z.; Wang, J. *Appl. Catal., A* **2009**, *365*, 62−70.
(98) Nickolov, R. N.; Edreva-Kardjieva, R.; Kafedjiysky, V. J.; Nikolova, D. A.; Stankova, N. B.; Mechandjiev, D. R. *Appl. Catal., A* **2000**, *190*, 191−196.
(99) Kantshewa, M.; Delannay, F.; Jeziorowski, H.; Delgado, E.; Eder, S.; Ertl, G.; Knozinger, H. *J. Catal.* **1984**, *87*, 482−496.
(100) Laniecki, M.; Malecka-Grycz, M.; Domka, F. *Appl. Catal., A* **2000**, *196*, 292−303.
(101) Jiang, M.; Bian, G.-Z.; Fu, Y.-L. *J. Catal.* **1994**, *146*, 144−154.
(102) Bao, J.; Sun, Z.-H.; Fu, Y.-L.; Bian, G.-Z.; Zhang, Y.; Tsubaki, N. *Top. Catal.* **2009**, *52*, 789−794.
(103) Rao, K. K.; Gravelle, M.; Valente, J. S.; Figueras, F. *J. Catal.* **1998**, *173*, 115−121.
(104) Cosimo, J. I. D.; Apesteguia, C. R.; Gines, M. J. L.; Iglesia, E. *J. Catal.* **2000**, *190*, 261−275.
(105) Carlini, C.; Flego, C.; Marchionna, M.; Noviello, M.; Galletti, A. M. R.; Sbrana, G.; Basile, F.; Vaccari, A. *J. Mol. Catal. A* **2004**, *220*, 215−220.
(106) Carlini, C.; Marchionna, M.; Noviello, M.; Galletti, A. M. R.; Sbrana, G.; Basile, F.; Vaccari, A. *J. Mol. Catal. A* **2005**, *232*, 13−20.
(107) Raybaud, P.; Hafner, J.; Kresse, G.; Kasztelan, S.; Toulhoat, H. *J. Catal.* **2000**, *189*, 129−146.
(108) Wambeke, L. A.; Jalowiecki, S.; Kasztelan, S.; Grimblot, J.; Bonnelle, J. P. *J. Catal.* **1988**, *109*, 320−328.
(109) Dumeignil, F.; Paul, J.; Veilly, E.; Qian, E.; Ishihara, A.; Payen, E.; Kabe, T. *Appl. Catal., A* **2005**, *289*, 51−58.
(110) Fan, Y.; Shi, G.; Liu, H.; Bao, X. *Appl. Catal., B* **2009**, *91*, 73−82.
(111) Sun, M.; Adjaye, J.; Nelson, A. E. *Appl. Catal., A* **2004**, *263*, 131−143.
(112) Cristol, S.; Paul, J. F.; Payen, E.; Bougeard, D.; Clémendot, S.; Hutschka, F. *J. Phys. Chem. B.* **2002**, *106*, 5659−5667.